Chemical Science

ROYAL SOCIETY OF CHEMISTRY

EDGE ARTICLE

View Article Online
View Journal | View Issue

Cite this: *Chem. Sci.*, 2026, **17**, 6109

All publication charges for this article have been paid for by the Royal Society of Chemistry

Carbon–iodine atropisomerism on triazole and triazolium frameworks: a breathing axle with divergent adaptivity

Ryoga Nambu,†[a] Jun Kikuchi, †*[a] Arimasa Matsumoto *[b] and Naohiko Yoshikai *[a]

Atropisomerism around a carbon–iodine(III) bond represents a rare form of chirality centered on a long, polarizable hypervalent linkage. Embedding this C–I(III) bond into an inherently asymmetric, diadamantylated triazole scaffold creates a vivid platform that reveals how such a bond responds to steric and electronic perturbations. Neutral triazole- and cationic triazolium–benziodoxoles display similarly high atropostability (racemization half-lives of several years at 25 °C), arising from opposing effects introduced by *N*-methylation: electronic weakening of the C–I bond *versus* steric buttressing that restricts rotation. Under acidic conditions, however, their behaviors diverge; the triazole derivative undergoes accelerated rotation, whereas the triazolium analogue retains substantial configurational stability. The CF_3 groups of the benziodoxole ring serve as sensitive ^{19}F NMR reporters for two complementary modes of chiral recognition. The neutral triazole engages BINOL through directional hydrogen bonding, whereas the triazolium derivative binds phosphate anions *via* halogen bonding and electrostatic interaction. Together, these results establish the hypervalent C–I(III) bond as a stereoelectronically tunable rotational element—an axle that enables molecular rotors combining well-defined rotational dynamics with switchable recognition behavior.

Received 18th December 2025
Accepted 26th January 2026

DOI: 10.1039/d5sc09936f

rsc.li/chemical-science

Introduction

Molecular motion is an inherent feature of chemical systems. Achieving control over such motion, even at the level of internal bond rotation, is a central objective in the design of functional molecules. From biphenyl rotors once used to gauge steric bulk[1,2] to the dynamic kinetic asymmetric transformations of configurationally fluxional biaryls[3–5] to the modern realm of molecular machines,[6,7] chemists have exploited and refined the control of restricted bond rotations through steric, electronic, acid–base, coordination, and even photoresponsive effects, thereby establishing hindered single bonds as design elements for functional molecular systems. These principles have been elaborated mainly for classical C–C and C–N atropisomers, and more recently for N–N, C–O, and C–B derivatives,[8] in which short, rigid bonds impose well-defined rotational barriers. Even simple yet fundamental stimuli—Brønsted and Lewis acid–base interactions—have inspired diverse molecular rotors, exemplified by a quinolyl imide,[9] a diarylamine,[10] and an arylborane, whose rotational dynamics are modulated by protonation or Lewis base coordination (Fig. 1a).[11] Extending the external stimuli-assisted control of bond rotation to heavier elements, whose bonds are intrinsically longer, more polarizable, and often associated with multiple accessible valence states, remains an unexplored area of stereochemical design. Atropisomerism about a C–S bond bearing moderately bulky aryl groups, whose asymmetry originates from sterically distinct *ortho* substituents (*t*Bu and Me), was reported to display racemization half-lives from minutes to several days depending on the internal sulfur valence state, *i.e.*, sulfide, sulfoxide, and sulfone (Fig. 1b);[12] however, this behavior arises from changes in intrinsic valence rather than from external chemical stimuli. Consequently, systematic strategies for achieving a high level of configurational stability together with externally controllable rotation of such and other classes of long bonds by deliberate ligand design remain in their infancy.[13] Beyond stereodynamic control, such chiral molecular systems—particularly those incorporating heavier elements, from the fourth row onward—may also offer access to unique properties and functions that originate from heavy-atom effects, including strong spin–orbit coupling, high polarizability, and pronounced anisotropy in noncovalent interactions.

The carbon–iodine(III) bond represents a distinctive case among atropisomeric systems, as it is markedly longer and

[a]*Graduate School of Pharmaceutical Sciences, Tohoku University, 6-3 Aoba, Aramaki, Aoba-ku, Sendai 980-8578, Japan. E-mail: jun.kikuchi.e8@tohoku.ac.jp; naohiko.yoshikai.c5@tohoku.ac.jp*

[b]*Department of Chemistry, Biology, and Environmental Sciences, Nara Women's University, Kita-Uoya Nishi-machi, Nara 630-8506, Japan. E-mail: a-matsumoto@cc.nara-wu.ac.jp*

† R. N. and J. K. contributed equally to this work.

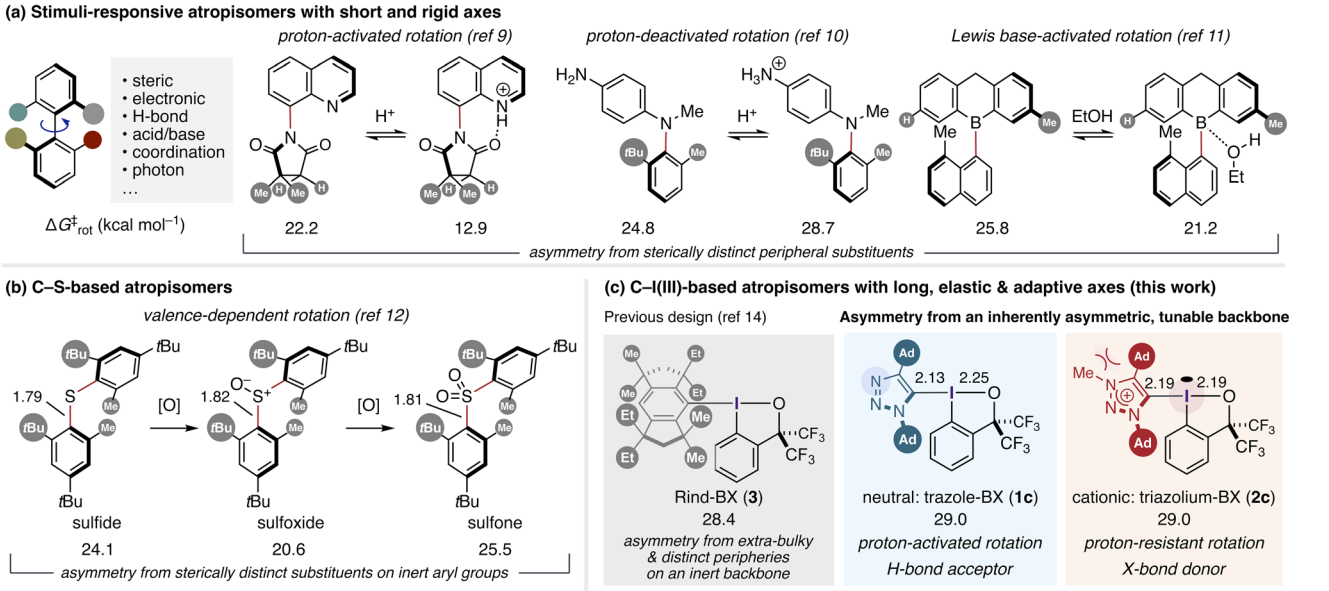

Fig. 1 Design space of atropisomers. (a) General concept and representative examples based on lighter elements, in which molecular asymmetry originates from different peripheral substituents. (b) C–S bond-based atropisomers relying on steric differentiation of *ortho*-substituents. (c) C–I(III) atropisomers enabled by an extremely bulky and unsymmetrical aryl group (previous work) and by decoupling molecular asymmetry from steric bulk, which opens channels for covalent and noncovalent modifications (this work).

more polar than the carbon–element bonds typically encountered in classical atropisomers.[14] Moreover, unlike ordinary two-center covalent bonds, its bond length and strength depend on both the carbon substituent and the *trans* ligand within the three-center four-electron hypervalent bonding framework.[15] Herein, we show that embedding this bond within an inherently asymmetric 1,2,3-triazole framework, supported by a benziodoxole (BX) scaffold, enables modulation of the rotational barrier and the stimuli-responsiveness of the C–I bond between the triazole ring and the trivalent iodine center through covalent modification of the triazole ring (Fig. 1c).

Flanked by twin adamantyl groups, both a neutral triazole and its cationic *N*-methyl triazolium form exhibit comparable levels of configurational stability at room temperature, as a result of opposing electronic and steric effects associated with *N*-methylation. The less electron-donating triazolium ligand leads to an elongated C–I bond, whereas the *N*-methyl group sterically enforces proximity of the adamantyl flank to the C–I bond. Under acidic conditions, however, their behaviors diverge markedly. The triazole derivative loses configurational stability by several orders of magnitude, whereas the triazolium analogue retains a significant rotational barrier. In addition to configurational stability and rotational dynamics, the two scaffolds exhibit complementary modes of chiral recognition. The neutral triazole-BX binds chiral donors such as BINOL *via* hydrogen bonding, whereas the cationic triazolium-BX recognizes chiral anions through halogen bonding at iodine.[16–19] Twin CF_3 groups in the BX scaffold serve as ^{19}F NMR probes,[20] enabling direct observation of these diastereomeric interactions as distinct sets of quartet signals. Collectively, these results demonstrate that the hypervalent C–I(III) bond serves as a stereoelectronically tunable axis,‡ enabling the design of heavy-atom atropisomers that integrate well-defined rotational dynamics with differentiated response and recognition behaviors.

Results and discussion

The realization of configurationally stable C–I atropisomerism is fundamentally difficult with common aryl frameworks, as in lighter-atom atropisomers (Fig. 1a and b). Indeed, in our previous study, an *ortho*-disubstituted aryl-BX bearing triisopropylsilyl and CF_3 substituents displayed a racemization half-life of only *ca.* 5 h, underscoring the intrinsic insufficiency of conventional aryl steric shielding around the C–I(III) axis.[14] This limitation was first overcome by extending the strategy of kinetic stabilization through extreme steric congestion to the atropisomeric C–I(III) bond. In this context, the exceptionally bulky Rind (1,1,3,3,5,5,7,7-octa-R-substituted *s*-hydrindacenyl) scaffold—originally developed to stabilize highly reactive main-group and organometallic species[21]—proved uniquely effective, enabling the synthesis and isolation of configurationally stable atropisomers such as **3** (Fig. 1c). This design, featuring sterically demanding yet structurally distinct groups on both *ortho* positions, was indispensable for effectively suppressing carbon–iodine(III) bond rotation while imparting chirality to the entire molecule. While effective, this strategy, which inherently couples steric bulk with molecular asymmetry, required multistep synthesis of each ligand, rendering systematic variation of steric demand and rotational barriers labor-intensive. Moreover, the scaffold does not readily permit post-functionalization or modulation by external chemical inputs. While the *trans* ligand, *i.e.*, benziodoxole oxygen, was demonstrated to function as a site for hydrogen-bond interaction to accelerate C–I bond

rotation and to enable chiral molecular recognition, the chemical inertness of the Rind ligand precluded systematic incorporation of additional covalent modifications or external stimuli into the atropisomeric framework. We therefore sought an alternative ligand framework that not only decouples molecular asymmetry from steric bulk but also offers a site for covalent and noncovalent modifications. The 1,2,3-triazole ring, readily accessible *via* Cu-catalyzed azide–alkyne cycloaddition (CuAAC),[22] was identified as a suitable platform to meet these criteria.

The synthesis of triazole-based benziodoxoles (**1a–1c**) was accomplished in a straightforward manner by CuAAC, lithiation, and trapping with chlorobenziodoxole (CBX) as the iodine(III) electrophile (Scheme 1). The three derivatives, with distinct steric environments at N(1) and C(4) (**1a**: N–Cy/C–C_8H_{17}; **1b**: N–Ad/C–TBS; **1c**: N–Ad/C–Ad), provided a simple series for probing the impact of substituent bulk on configurational stability. As anticipated, rotation about the C–I(III) bond—quantified by the rotational free-energy barrier ($\Delta G^{\ddagger}_{rot}$) and the corresponding racemization half-life ($t_{1/2}$ *rac*) at 25 °C—was fastest for **1a** (17.8 kcal mol^{-1}, 1.2 s) and progressively slowed for **1b** (25.9 kcal mol^{-1}, 12.5 days) and **1c** (29.0 kcal mol^{-1}, 6.4 years). According to LaPlante's widely used classification[23,24]—Class 1 (<minutes), Class 2 (hours–days), and Class 3 (>years)—these three members of the series fall cleanly into Class 1, Class 2, and Class 3, respectively. This explicitly demonstrates that the triazole framework, despite its synthetic simplicity, spans the full spectrum of atropisomeric behavior defined by LaPlante. The pseudosymmetric, doubly adamantylated species **1c**, in particular, attains a level of stability comparable to Rind scaffolds such as **3**, demonstrating the effectiveness of the ligand design strategy that decouples skeletal asymmetry from steric bulk imposed by peripheral substituents. Attempts to install other benziodoxol(on)e scaffolds into the bulkiest triazole framework did not yield atropisomers amenable to optical resolution, consistent with our recent observation of the unique stability of the bis(trifluoromethyl)-based BX scaffold.[25]

Encouraged by the high configurational stability of the doubly adamantylated triazole-BX **1c**, we introduced an electronic perturbation to this rigid framework. Methylation of the triazole nitrogen with methyl triflate cleanly furnished the corresponding triazolium-BX **2c** in excellent yield (Scheme 1). Despite the positive charge introduced onto the triazole ring, **2c** retained nearly identical configurational stability to **1c** ($\Delta G^{\ddagger}_{rot}$ = 29.0 kcal mol^{-1}; $t_{1/2}$ *rac* (25 °C) = 6.4 years). This parity in atropostability between the neutral and cationic states cannot be accounted for solely by the well-known buttress effect in atropisomeric systems, as the *N*-methyl group of **2c** would be expected to push the C(4)-adamantyl substituent toward the C–I bond, thereby increasing the rotational barrier.

Despite their nearly identical rotational barriers, the crystal structures of **1c** and **2c** revealed important structural differences around the C–I(III) bond of these atropisomers (Fig. 2). Neutral **1c** crystallizes in a pseudo-symmetric, disordered form, its triazole ring occupying two opposite orientations with equal probability—an expression of its near-perfect steric symmetry. This disorder arises from the near-equivalence of its two adamantyl flanks and does not obscure the identity of the iodine-bearing carbon, yet it limits the precision with which internal ring metrics can be interpreted. The most reliable indicators—the apical bond lengths—show a typical λ^3-iodane geometry (C–I = 2.13 Å, I–O = 2.25 Å). Upon *N*-methylation, this pseudosymmetry is broken, yielding a single, ordered structure in which the triazolium ring exerts a distinct electronic and steric influence. The C–I bond elongates (2.19 Å), while the *trans* I–O bond shortens (2.19 Å), reflecting the *trans* influence:[15,26,27] the cationic triazolium carbon donates less to iodine, and the benziodoxole oxygen compensates by drawing closer. Meanwhile, the newly installed *N*-methyl group presses against the

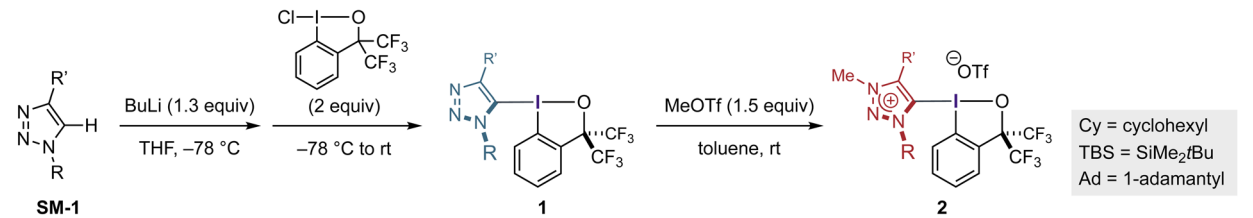

compound (yield)	**1a** (99%)	**1b** (53%)	**1c** (54%)	**2c** (92%)	**3**
$\Delta G^{\ddagger}_{rot}$ (kcal mol^{-1})	17.8	25.9	29.0	29.0	28.4
$t_{1/2}$ *rac* (25 °C)	1.2 s	12.5 d	6.4 y	6.4 y	2.3 y
atropisomer class	*Class 1*	*Class 2*	*Class 3*	*Class 3*	*Class 3*

Scheme 1 Synthesis of triazole-BXs **1a–1c** and triazolium-BX **2c** and determination of their rotational barriers and racemization half-lives (DMSO-d_6 for **1a**, CH_2Cl_2 for **1b**, toluene for **1c** and **3**, chlorobenzene for **2c**). See the SI for the details of synthetic procedures and kinetic measurements.

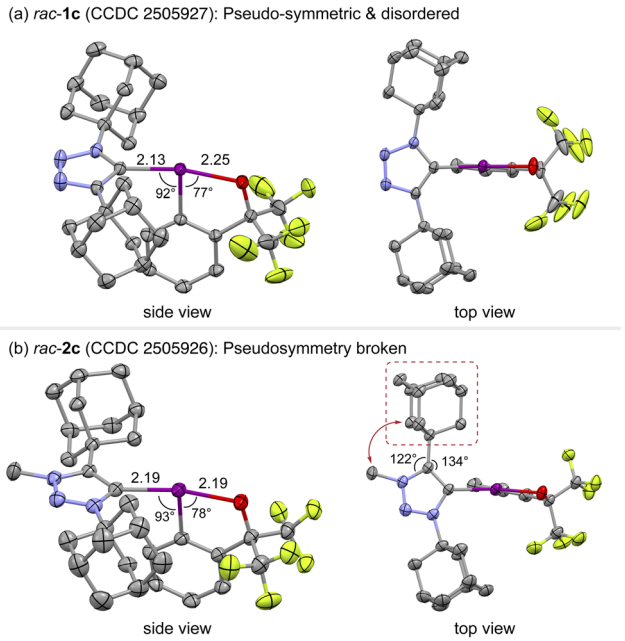

Fig. 2 ORTEP diagrams of (a) *rac*-**1c** and (b) *rac*-**2c** with thermal ellipsoids set to 50% probability. A single molecule is extracted from the unit cell, and solvent molecules and OTf anion (for *rac*-**2c**) are omitted for clarity. See the SI for the details of the disorder of *rac*-**1c**.

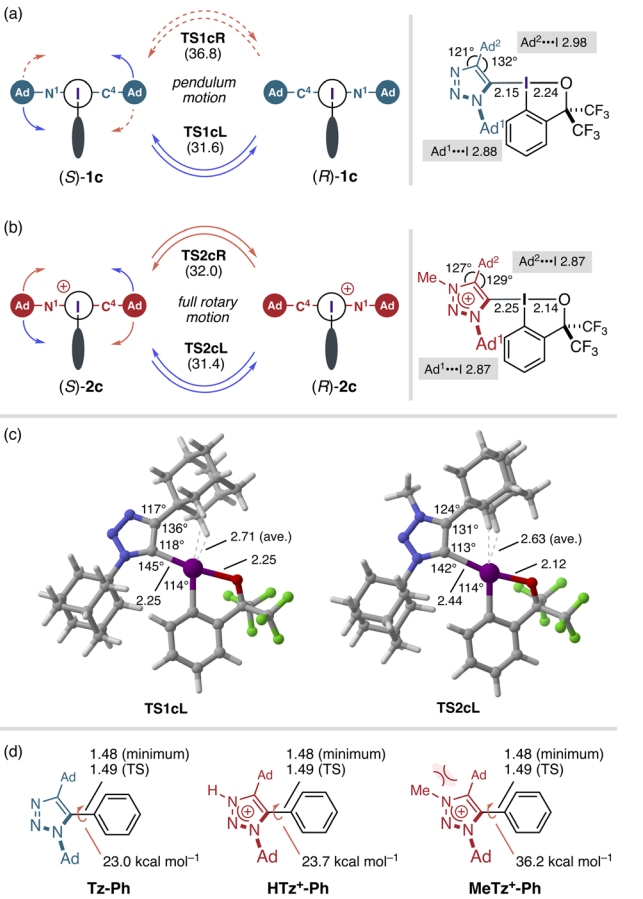

Fig. 3 DFT calculations (M06-2X(SMD,toluene)/6-311+G(2df,2p)-SDD(for I)//M06-2X/6-31+G(d,p) SDD(for I)). (a and b) Rotatory behaviors of **1c** and **2c** and the summary of their ground-state structures. Activation free energies (in kcal mol^{-1}) are given in parentheses. Ad^1···I and Ad^2···I refer to the average of the two shortest H–I distances of the respective adamantyl groups. (c) 3D structures of TS1cL and TS2cL. (d) Summary of calculated structures and C–C rotational barriers of triazole-phenyl and triazolium-phenyl species.

adjacent adamantyl substituent, twisting the C(4)–Ad vector to relieve an allylic-like 1,3-interaction. These structural features indicate the coexistence of electronic weakening and steric buttressing in the triazolium-BX **2c** in the solid state.

Density functional theory (DFT) calculations were performed to elucidate the enantiomerization pathway and the structural factors governing the rotational barriers of **1c** and **2c** by evaluating both clockwise and counterclockwise rotation around the C–I bond, starting from the *S*-configured enantiomers (Fig. 3a and b; see also Fig. S24). For both molecules, the counterclockwise pathway proved energetically favored, with calculated activation free energies ($\Delta G^{\ddagger}$ = 31.6 kcal mol^{-1} for **1c**; 31.4 kcal mol^{-1} for **2c**) in reasonable agreement with the experimental values (29.0 kcal mol^{-1} for both). In all transition states (TSs), the iodine(III) center exhibited a pronounced deviation from the ideal T-shaped geometry. To alleviate steric repulsion between the adamantyl substituents and the benziodoxole (BX) aromatic ring, the C–I–C and adjacent I–C–X (X = N or C) angles expanded significantly and the C–I bond underwent elongation by up to 10%, thereby generating substantial strain energy that elevates the rotational barrier—behavior reminiscent of that previously observed in the Rind-BX system (Fig. 3c).[14] This angular deformation inevitably drags the "remote" adamantyl substituent toward the iodine center, so that both substituents become sterically engaged in the TS even along the apparently more open pathway. Notably, **1c** displayed a distinct asymmetry between the two rotational pathways. The clockwise rotation (**TS1cR**), in which the C(4)-adamantyl group sweeps across the BX ring, incurred a higher barrier ($\Delta G^{\ddagger}$ = 36.8 kcal mol^{-1}) than the counterclockwise counterpart (**TS1cL**, 31.6 kcal mol^{-1}), reflecting the greater dihedral distortion (see Fig. S24). This energetic imbalance implies that racemization of **1c** proceeds effectively through a single, lower-energy half-rotation—rendering the molecule a pendulum-type rotor rather than a free one. In contrast, **2c** exhibited nearly degenerate pathways ($\Delta G^{\ddagger}$ = 31.4 and 32.0 kcal mol^{-1}), pointing to a rotary-type racemization profile. Consistent with the inference from X-ray analysis, *N*-methylation elongates the C–I bond in both the ground state and TS, while widening the N(3)–C(4)–Ad angle. The latter introduces a buttressing effect,[28–30] wherein steric repulsion between the methyl and adamantyl groups pushes the latter toward the iodine center. This additional steric reinforcement counterbalances the nominal barrier-lowering effect of C–I(III) bond elongation and thereby maintains the high barrier of **2c**. These calculations clarify how steric buttressing and C–I bond elongation are manifested differently in the enantiomerization dynamics of **1c** and **2c**.

To delineate the unique behavior of the hypervalent C–I bond as a rotating axis, we performed parallel calculations on

the corresponding C–C analogues (**Tz-Ph**, **HTz$^+$-Ph**, and **MeTz$^+$-Ph**), in which the benziodoxole moiety was replaced by a phenyl group (Fig. 3d). In these reference systems, the triazole–phenyl and triazolium–phenyl bonds exhibited nearly identical C–C distances in both the ground and transition states (1.48–1.49 Å) and showed little response to either *N*-protonation or *N*-methylation. Yet their rotational profiles diverged sharply: neutral **Tz-Ph** and protonated **HTz$^+$-Ph** exhibited comparable barriers of 23–24 kcal mol^{-1}, whereas the methylated **MeTz$^+$-Ph** required a markedly higher barrier of 36.2 kcal mol^{-1}. This steep rise reflects the buttress effect of the *N*-methyl group, which cannot be mitigated within the rigid C–C framework. By contrast, the C–I bond and the surrounding bond angles in the BX systems act collectively as a flexible joint, lengthening and bending significantly between the ground and transition states as well as between neutral and cationic forms (shortest in **1c** at 2.15 Å; longest in **TS2cL** at 2.44 Å) to alleviate steric repulsion. Such flexibility enables dynamic compensation between electronic withdrawal (by *N*-methylation) and steric reinforcement (by the methyl group). The comparable atropostability **1c** and **2c** is therefore not coincidental but emerges from the elastic nature of hypervalent bonding, a feature that is largely absent in two-center covalent bonds.

The configurational stability of **1c** and **2c** was next examined under acidic conditions (Fig. 4). Enantioenriched **1c** displayed essentially equal atropostability in non-protic or coordinating media such as toluene, chlorobenzene, THF, and triethylamine ($\Delta G^{\ddagger}_{rot} \approx 29$ kcal mol^{-1}), but underwent rapid racemization upon exposure to acids (Fig. 4a). In acetic acid, the barrier fell to 25.3 kcal mol^{-1} ($t_{1/2}$ *rac* (25 °C) = 4.5 days), and addition of 1 equiv TFA in toluene further reduced it to 23.6 kcal mol^{-1} ($t_{1/2}$ *rac* (25 °C) < 7 h). In sharp contrast, **2c** showed only muted responses under the same acidic conditions ($\Delta G^{\ddagger}_{rot} \approx 27.5$–28.7 kcal mol^{-1}, $t_{1/2}$ *rac* (25 °C) ≈ 0.51–3.9 years). Comparison with the Rind-BX benchmark **3** clarifies this divergence. Compound **3** displays a pronounced drop in barrier ($\Delta\Delta G^{\ddagger}$ > 6 kcal mol^{-1}) when moving from toluene (28.4 kcal mol^{-1}) to acetic acid (22.2 kcal mol^{-1}) or to TFA-containing media (21.9 kcal mol^{-1}). This behavior reflects *O*-activation: hydrogen bonding to the BX oxygen weakens the I–O interaction and enhances the conformational flexibility of the hypervalent scaffold, allowing the C–I–C angle and the aryl–iodine axis to undergo the required transition-state deformations with reduced distortion energy (Fig. 4b).[14] In **1c**, however, the pattern differs. It shows a moderate response to acetic acid ($\Delta\Delta G^{\ddagger} \approx$ 3.7 kcal mol^{-1}) but a drop comparable to **3** upon TFA addition ($\Delta\Delta G^{\ddagger} \approx 5.4$ kcal mol^{-1}). This split behavior suggests a distinct mode of accelerated rotation. Rather than *O*-activation, the rotation of **1c** would be accelerated *via N*-activation of the triazole, wherein hydrogen bonding or partial protonation at N(3) electronically elongates the C–I bond (Fig. S25). This acid-strength-dependent elasticity may reflect a graded response of the rotational barrier to protonic strength. Meanwhile, the acid-resistant configurational stability of **2c** may be ascribed to two plausible reasons. In nonpolar PhCl, **2c** forms a contact ion pair in which the triflate anion occupies the σ-hole region opposite iodine (as also seen crystallographically; Fig. S7), electrostatically blocking the BX oxygen toward protonic activation by TFA. In acetic acid, the ion pair is expected to loosen into a solvent-separated ion pair due to triflate solvation; however, the cationic triazolium unit pulls the BX oxygen toward iodine, rendering it less basic and preventing the O–H hydrogen bonding that would increase the conformational flexibility of the hypervalent scaffold. Thus, acids influence the rotational behavior of the C–I(III) bond through different mechanisms—*O*-activation for **3**, *N*-activation for **1c**, and electrostatic shield for **2c**—highlighting the electronic susceptibility of the C–I(III) axis as a design element of molecular rotors.

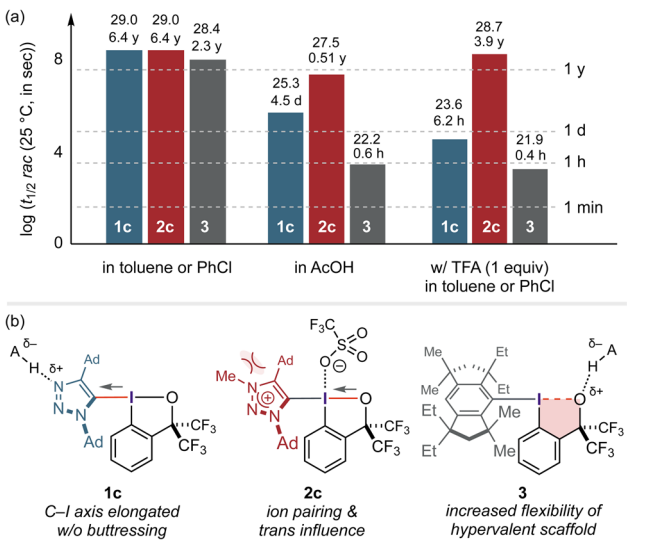

Fig. 4 Response of **1c**, **2c**, and **3** to acids. (a) Comparison of racemization half-lives (at 25 °C) of these compounds under different conditions on a log scale. Above each bar are shown the half-life in a convenient timescale and the activation energy in kcal mol^{-1}. (b) Schematic rationale for the compound-characteristic acid response.

The divergent electronic structures of **1c** and **2c** give rise to distinct modes of chiral molecular recognition, reflected in the ^{19}F NMR response of the CF_3 groups of the BX moiety (Fig. 5).[20] When (*R*)-BINOL was added to racemic **1c** in toluene-d_8, the CF_3 quartet of the BX ring split into two discrete sets, indicating the formation of diastereomeric hydrogen-bonded adducts between the neutral triazole-BX and the chiral alcohol. Enantioenriched (+)- and (−)-**1c** each produced a single quartet pair at mirror-related positions, and overlaying the two spectra reproduced the pattern of the racemic mixture, confirming direct enantiodifferentiation of **1c** through hydrogen-bond-mediated recognition. By contrast, addition of (*R*)-BINOL to **2c** resulted only in minor broadening and slight splitting of the quartet pair (Fig. S21), without the clear peak separation observed for **1c**, consistent with the diminished hydrogen-bond-accepting ability of the triazolium unit. Notably, even the archetypal Rind-BX **3**, which is known to engage in hydrogen bonding, showed only a faint signal perturbation under identical conditions. This comparison highlights the uniquely effective hydrogen-bond-acceptor character of the triazole unit in **1c**, where directional N(3) coordination is optimally coupled to the configurationally rigid C–I(III) axis.

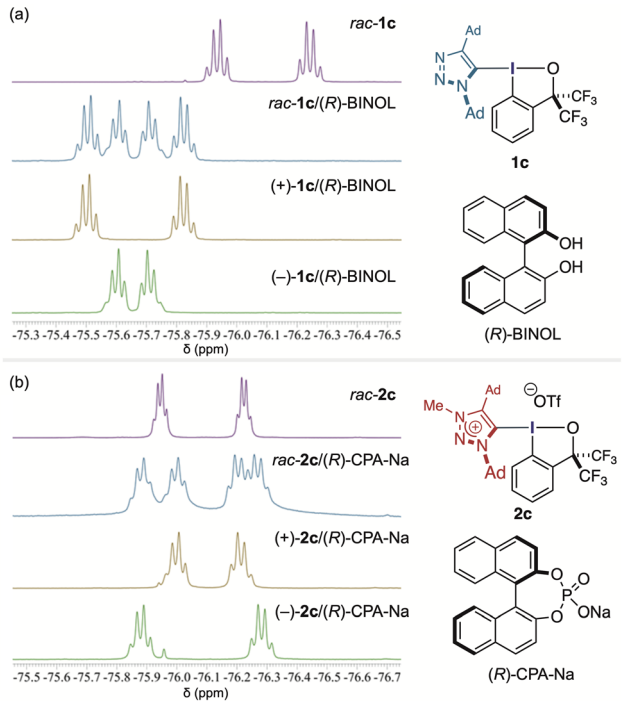

Fig. 5 ^{19}F NMR spectra illustrating chiral recognition of triazole- and triazolium-BXs: (a) **1c** with (*R*)-BINOL and (b) **2c** with (*R*)-CPA–Na.

In contrast, the triazolium-BX **2c** exhibited a distinct mode of chiral recognition. Addition of the anionic (*R*)-CPA–Na salt induced splitting of the ^{19}F NMR signals, consistent with the formation of diastereomeric ion-paired complexes. This recognition originates from halogen bonding between the σ-hole on iodine(III) and the oxygen atoms of the phosphate anion, reinforced by coulombic attraction within the contact ion pair. Under identical conditions, addition of (*R*)-CPA–Na to **1c** caused no discernible change in the CF_3 quartet pattern, indicating the absence of measurable chiral discrimination (Fig. S21). The halogen-bonding ability of **2c** was quantified by ^{31}P NMR using triethylphosphine oxide as a probe (Fig. S22).[31] The pronounced downfield shift observed for **2c** ($\Delta\delta$ = 19.6 ppm) far exceeded those of **3** (0.22 ppm), **1c** (0.60 ppm), and typical aryl iodides, identifying **2c** as a distinctly stronger halogen-bond donor. Consistent with this enhanced σ-hole character, **2c** also displayed modest activity in a halogen-bond-promoted quinoline reduction with a Hantzsch ester (Table S3). Taken together with the hydrogen-bond-mediated recognition observed for **1c**, these results demonstrate that neutral and cationic triazole-BX atropisomers exhibit complementary modes of molecular recognition, arising from deliberate modification of the hypervalent C–I(III) bond.

Conclusions

In conclusion, we have synthesized configurationally stable and stimuli-responsive carbon–iodine(III) atropisomers in which bulky, diadamantylated triazole and triazolium groups are directly linked to a benziodoxole scaffold. Although the neutral and cationic derivatives exhibit similarly high levels of atropostability, their responses to external stimuli diverge markedly. Taken together, the pronounced elongation, polarity modulation, and stimulus-dependent behavior of the hypervalent C–I(III) bond define a "breathing" atropisomeric axis—one whose structural and stereoelectronic parameters undergo coordinated, reversible adjustment across multiple perturbations. The neutral triazole derivative undergoes accelerated rotation under protonic activation and engages in hydrogen-bond-mediated recognition with BINOL, whereas the triazolium analogue retains its configurational stability under acidic conditions while recognizing anionic guests through halogen bonding and electrostatic interaction. The comparable thermal atropostability of the two systems can be rationalized by a balance between opposing steric and electronic effects acting on the hypervalent C–I(III) bond. *N*-methylation introduces steric reinforcement while simultaneously elongating and electronically weakening the C–I bond, leading to an effective compensation of these effects. Such adaptive modulation of bond length, polarity, and rotational resistance is not observed in conventional atropisomers based on short, rigid, two-center covalent bonds of lighter elements. Together, these results demonstrate that the carbon–iodine(III) bond—traditionally employed either as a transient linkage in molecular transformations or as a static σ-hole donor in halogen bonding[32–35]—can serve as a stereoelectronically tunable axle for molecular rotors within a rationally designed hypervalent framework. In the present study, bulky triazole groups are established as effective design elements, alongside Rind frameworks, for accessing otherwise challenging heavy-atom atropisomers with tangible configurational stability. Beyond the present C–I atropisomers, the inherently asymmetric and synthetically modular triazole framework provides a general platform for the construction of broader and more complex atropisomeric architectures, including multiaxial systems centered on carbon–iodine(III) bonds as well as extension to new classes of heavy-atom atropisomers. These directions, enabled by the decoupling of skeletal asymmetry from steric bulk, are currently being pursued in our laboratories.

Author contributions

Ryoga Nambu: investigation; data curation. Jun Kikuchi: conceptualization; investigation; formal analysis; writing – original draft; writing – review & editing; funding acquisition. Arimasa Matsumoto: investigation; formal analysis. Naohiko Yoshikai: conceptualization; writing – review & editing; supervision; project administration; funding acquisition.

Conflicts of interest

There are no conflicts to declare.

Data availability

CCDC 2505926 (**2c**) and 2505927 (**1c**) contain the supplementary crystallographic data for this paper.[36a,b]

The data supporting this article have been included as part of the supplementary information (SI). Supplementary information: Fig. S1–S39, Tables S1–S4, and further experimental and computational details. See DOI: https://doi.org/10.1039/d5sc09936f.

Acknowledgements

This work was supported by JSPS KAKENHI (Grant No. JP24K01478 (N. Y.) and JP24K17665 (J. K.)), Asahi Glass Foundation (N. Y.), Naito Foundation (N. Y.), Daiichi Sankyo Foundation of Life Science (N. Y.), Toyota Riken Scholar Program (J. K.), the Foundation for the Promotion of Ion Engineering (J. K.), and Research Support Project for Life Science and Drug Discovery (Basis for Supporting Innovative Drug Discovery and Life Science Research (BINDS)) from AMED (Grant No. JP25ama121040 (N. Y.)). We thank Central Glass Co., Ltd for the generous donation of 1,1,1,3,3,3-hexafluoro-2-phenylpropan-2-ol (HFAB).

Notes and references

‡ In this paper, axis refers to the stereogenic C–I(III) bond itself (structural context), whereas axle is used only when describing its rotor-like or adaptive functional behavior. This distinction mirrors common usage in the molecular machines literature and avoids conflation between structural and functional terminology.

1 R. Adams and H. C. Yuan, *Chem. Rev.*, 1933, **12**, 261–338.
2 H. Förster and F. Vögtle, *Angew. Chem., Int. Ed. Engl.*, 1977, **16**, 429–441.
3 C. B. Roos, C.-H. Chiang, L. A. M. Murray, D. Yang, L. Schulert and A. R. H. Narayan, *Chem. Rev.*, 2023, **123**, 10641–10727.
4 J. Zhang, X. Huo, Y. Liu and C. Zhu, *Chem Catal.*, 2025, **5**, 101329.
5 G. Ma and M. P. Sibi, *Chem.–Eur. J.*, 2015, **21**, 11644–11657.
6 G. S. Kottas, L. I. Clarke, D. Horinek and J. Michl, *Chem. Rev.*, 2005, **105**, 1281–1376.
7 A. Mondal, R. Toyoda, R. Costil and B. L. Feringa, *Angew. Chem., Int. Ed.*, 2022, **61**, e202206631.
8 G.-J. Mei, W. L. Koay, C.-Y. Guan and Y. Lu, *Chem*, 2022, **8**, 1855–1893.
9 B. E. Dial, P. J. Pellechia, M. D. Smith and K. D. Shimizu, *J. Am. Chem. Soc.*, 2012, **134**, 3675–3678.
10 Y. Iwasaki, R. Morisawa, S. Yokojima, H. Hasegawa, C. Roussel, N. Vanthuyne, E. Caytan and O. Kitagawa, *Chem.–Eur. J.*, 2018, **24**, 4453–4458.
11 T. H. Doan, A. Chardon, N. Vanthuyne, T. N. Ramos, N. Tumanov, L. Fusaro, M. Albalat, L. Collard, J. Wouters, B. Champagne and G. Berionni, *Angew. Chem., Int. Ed.*, 2025, **64**, e202421931.
12 J. Clayden, J. Senior and M. Helliwell, *Angew. Chem., Int. Ed.*, 2009, **48**, 6270–6273.
13 T. A. Schmidt, S. Schumann, A. Ostertag and C. Sparr, *Angew. Chem., Int. Ed.*, 2023, **62**, e202302084.
14 S. Abe, J. Kikuchi, A. Matsumoto and N. Yoshikai, *Chem*, 2025, **11**, 102527.
15 M. Ochiai, T. Sueda, K. Miyamoto, P. Kiprof and V. V. Zhdankin, *Angew. Chem., Int. Ed.*, 2006, **45**, 8203–8206.
16 G. Cavallo, P. Metrangolo, R. Milani, T. Pilati, A. Priimagi, G. Resnati and G. Terraneo, *Chem. Rev.*, 2016, **116**, 2478–2601.
17 A. Brown and P. D. Beer, *Chem. Commun.*, 2016, **52**, 8645–8658.
18 P. Politzer, J. S. Murray and T. Clark, *Phys. Chem. Chem. Phys.*, 2013, **15**, 11178–11189.
19 D. Jovanovic, M. P. Mohanan and S. M. Huber, *Angew. Chem., Int. Ed.*, 2024, **63**, e202404823.
20 Z. Xu and Y. Zhao, *Chem. Rec.*, 2023, **23**, e202300031.
21 T. Matsuo and K. Tamao, *Bull. Chem. Soc. Jpn.*, 2015, **88**, 1201–1220.
22 M. Meldal and C. W. Tornøe, *Chem. Rev.*, 2008, **108**, 2952–3015.
23 S. R. LaPlante, P. J. Edwards, L. D. Fader, A. Jakalian and O. Hucke, *ChemMedChem*, 2011, **6**, 505–513.
24 S. R. LaPlante, L. D. Fader, K. R. Fandrick, D. R. Fandrick, O. Hucke, R. Kemper, S. P. F. Miller and P. J. Edwards, *J. Med. Chem.*, 2011, **54**, 7005–7022.
25 B. Li, J. Kikuchi, A. Matsumoto and N. Yoshikai, *Chem. Lett.*, 2025, **54**, upaf199.
26 P. K. Sajith and C. H. Suresh, *Inorg. Chem.*, 2012, **51**, 967–977.
27 P. K. Sajith and C. H. Suresh, *Inorg. Chem.*, 2013, **52**, 6046–6054.
28 M. Rieger and F. H. Westheimer, *J. Am. Chem. Soc.*, 1950, **72**, 19–28.
29 G. Bott, L. D. Field and S. Sternhell, *J. Am. Chem. Soc.*, 1980, **102**, 5618–5626.
30 G. Bringmann, A. J. P. Mortimer, P. A. Keller, M. J. Gresser, J. Garner and M. Breuning, *Angew. Chem., Int. Ed.*, 2005, **44**, 5384–5427.
31 Y. P. Chang, T. Tang, J. R. Jagannathan, N. Hirbawi, S. Sun, J. Brown and A. K. Franz, *Org. Lett.*, 2020, **22**, 6647–6652.
32 A. Yoshimura and V. V. Zhdankin, *Chem. Rev.*, 2016, **116**, 3328–3435.
33 D. P. Hari, P. Caramenti and J. Waser, *Acc. Chem. Res.*, 2018, **51**, 3212–3225.
34 A. Yoshimura and V. V. Zhdankin, *Chem. Rev.*, 2024, **124**, 11108–11186.
35 X. Peng, A. Rahim, W. Peng, F. Jiang, Z. Gu and S. Wen, *Chem. Rev.*, 2023, **123**, 1364–1416.
36 (*a*) CCDC 2505926 (**2c**): Experimental Crystal Structure Determination, 2026, DOI: 10.5517/ccdc.csd.cc2q3mbt; (*b*) CCDC 2505927 (**1c**): Experimental Crystal Structure Determination, 2026, DOI: 10.5517/ccdc.csd.cc2q3mcv.